ACS APPLIED MATERIALS & INTERFACES

Research Article

www.acsami.org

Insight into the Effect of Boron Doping on Sulfur/Carbon Cathode in Lithium–Sulfur Batteries

Chun-Peng Yang, Ya-Xia Yin, Huan Ye, Ke-Cheng Jiang, Juan Zhang, and Yu-Guo Guo*

CAS Key Laboratory of Molecular Nanostructure and Nanotechnology and Beijing National Laboratory for Molecular Sciences, Institute of Chemistry, Chinese Academy of Sciences (CAS), Beijing 100190, P. R. China

Supporting Information

ABSTRACT: To exploit the high energy density of lithium–sulfur batteries, porous carbon materials have been widely used as the host materials of the S cathode. Current studies about carbon hosts are more frequently focused on the design of carbon structures rather than modification of its properties. In this study, we use boron-doped porous carbon materials as the host material of the S cathode to get an insightful investigation of the effect of B dopant on the S/C cathode. Powder electronic conductivity shows that the B-doped carbon materials exhibit higher conductivity than the pure analogous porous carbon. Moreover, by X-ray photoelectron spectroscopy, we prove that doping with B leads to a positively polarized surface of carbon substrates and allows chemisorption of S and its polysulfides. Thus, the B-doped carbons can ensure a more stable S/C cathode with satisfactory conductivity, which is demonstrated by the electrochemical performance evaluation. The S/B-doped carbon cathode was found to deliver much higher initial capacity (1300 mA h g^{-1} at 0.25 C), improved cyclic stability, and rate capability when compared with the cathode based on pure porous carbon. Electrochemical impedance spectra also indicate the low resistance of the S/B-doped C cathode and the chemisorption of polysulfide anions because of the presence of B. These features of B doping can play the positive role in the electrochemical performance of S cathodes and help to build better Li–S batteries.

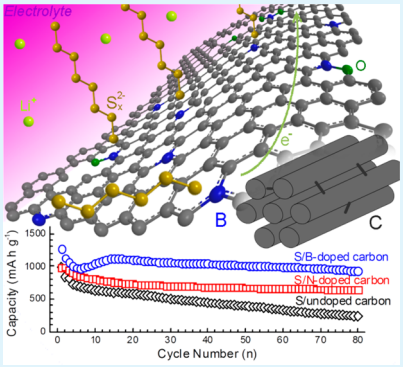

KEYWORDS: *batteries, lithium–sulfur batteries, sulfur/carbon composite, boron doping, electrochemical properties*

1. INTRODUCTION

The explosive growth in demand for high energy density devices has prompted the intense efforts toward development of various energy storage materials.[1−4] Lithium–sulfur batteries have been considered to be promising energy storage devices and have attracted considerable attention over the years.[5] The high theoretical capacity of S (1675 mA h g^{-1}) enables the Li–S batteries to provide a theoretical energy density of approximately 2600 W h kg^{-1}, which is much higher than that of conventional Li-ion batteries.[6] Moreover, S is abundant, inexpensive, and nontoxic, which makes it a prospective choice for wide applications. Despite these advantages, practical applications of Li–S batteries are still plagued with many challenges.[7] One such major issue is the insulating nature of S and its reduced product Li_2S, leading to low utilization of the active material and inferior rate capability. Another problem is the intermediate polysulfide species formed during cycling, which are soluble in the electrolyte and shuttle between the electrodes. This phenomenon, known as "shuttle effect", results in a low Coulombic efficiency and poor cycling life of the battery.

Multiple strategies of cathode design have been developed to address these issues, among which encapsulation of S in conductive host materials has proven to be fruitful.[8,9] The conductive host materials can provide the conducting network while retarding the dissolution of polysulfides, thereby contributing to high capacity and favorable cycle life of the cathode. Because of the high conductivity and low density of carbon, various carbon materials have been used as the hosts for S and significantly improve the cathode performance.[10−27] However, most reported investigations with S/C cathodes are focused on the structure design, such as tuning the pore size,[10,11] varying the pore shapes,[12−15] exploring various nanostructured carbon materials,[14−18] and building hierarchical or other complex architectures.[19] In fact, besides the structural characteristics, intrinsic properties of carbon including surface chemistry, electronic conductivity, and surface polarization are also critical for the S/C cathode and its reduced counterpart.[28,29] So far, research regarding these aspects is sparse and limited.

A successful approach to modifying the intrinsic properties of pure carbon is by doping with heteroatoms, such as N, B, S, and P.[30] Doping carbons by N has been by far the most widely investigated and yields a thriving class of N-doped carbon materials with various applications, including Li-ion batteries.[30−34] In Li–S batteries, N-doped carbons have been reported to exhibit improved conductivity and enhance the activity of S.[35,36] B, electron-deficient counterpart to N, is

Received: March 17, 2014
Accepted: April 15, 2014
Published: April 15, 2014

   dx.doi.org/10.1021/am501627f | ACS Appl. Mater. Interfaces 2014, 6, 8789–8795

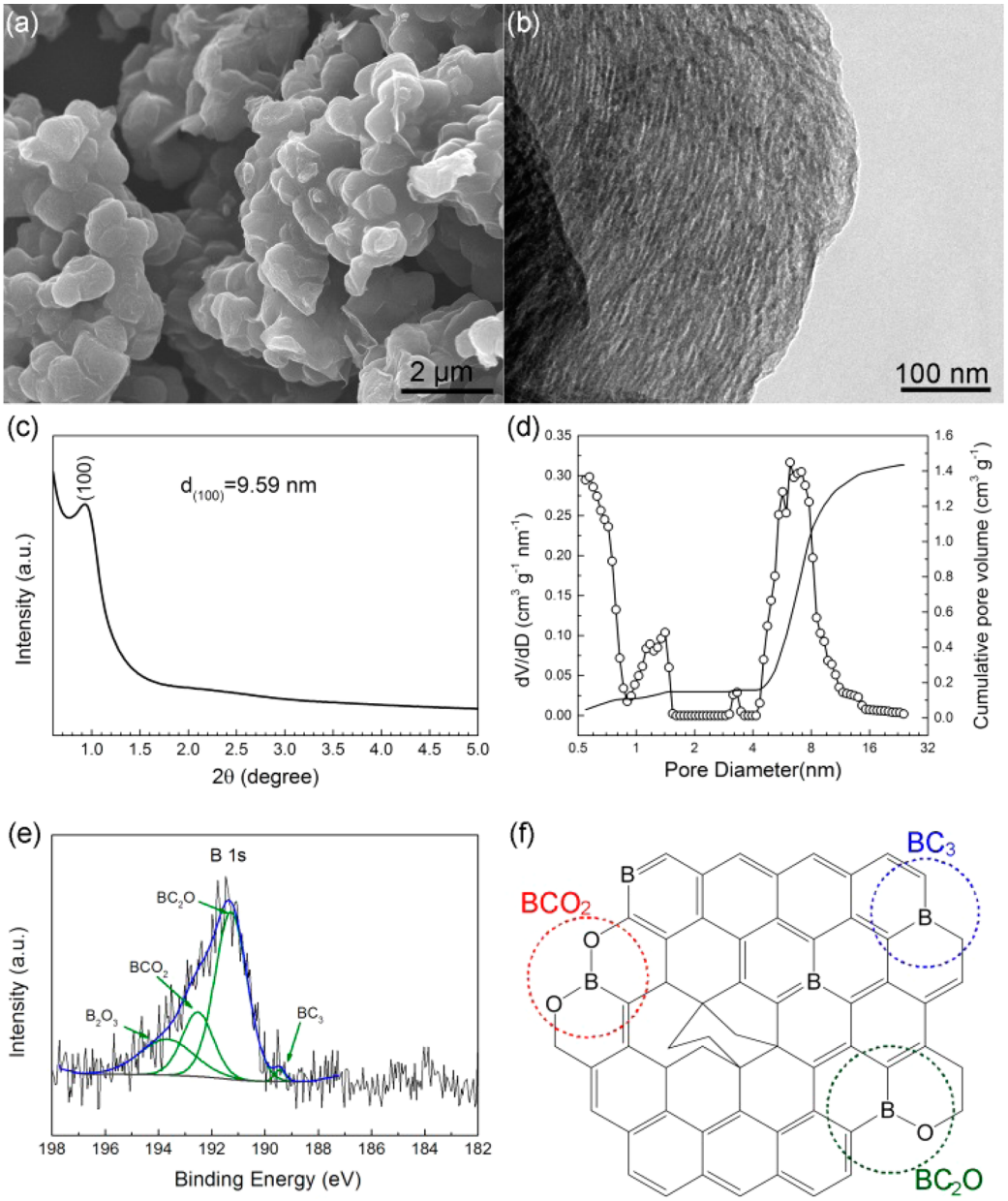

Figure 1. (a) SEM and (b) TEM image of BPC; (c) low-angle XRD pattern of BPC; (d) pore size distribution and cumulative pore volume of BPC; (e) B 1s XPS analysis for BPC; (f) schematic illustration of different B-containing functional groups in carbon backbone based on the XPS analysis in (e).

another prospective dopant.[37−39] On one hand, B-doped carbon has higher conductivity than plain carbon, much like that of N-doped carbon. On the other hand, in contrast to N-doped carbon, B dopant in the carbon framework is positively polarized, leading to chemisorption with negatively charged species.[37] Thus, B-doped carbons are expected to attract polysulfide anions, thereby alleviating the shuttle effect.

Herein, we gain an insight into the role of B dopant on S/C cathode by using B-doped porous carbon (BPC) as the host material for S. Our study shows that because of the synergy between B, C, and S, doping with B remarkably improves the conductivity of the crude porous carbon and alters its surface properties to effectively trap the polysulfide anions. Therefore, S/BPC cathode shows high capacity, stable cyclability, and excellent rate capability.

2. EXPERIMENTAL SECTION

2.1. Synthesis. *Synthesis of Carbon Materials.* Silica template SBA-15 was synthesized as described in a previous publication[40] and then used as the hard template for porous carbon synthesis. BPC was prepared via a method developed from the synthesis of ordered mesoporous carbon CMK-3.[12,38,40] For the synthesis of BPC, 1 g of boric acid (Beijing Chemical Works) was first dissolved in 5 mL of deionized water by sonication and heating. Then 1 g of D-fructose (Aladdin Industrial Inc.) and 0.14 g of concentrated H_2SO_4 were dissolved in the above solution, followed by addition of 1.0 g of SBA-15 and sonication for 1 h. The mixture was heated at 100 °C for 12 h and at 160 °C for another 12 h, followed by repetition of the impregnation process with another 5 mL of aqueous solution containing 0.8 g of boric acid, 0.8 g of D-fructose, and 0.09 g of H_2SO_4. The obtained dark brown intermediate product was completely carbonized at 900 °C for 5 h in an Ar flow. To remove the SBA-15 template, the carbonized product was stirred in 2 M

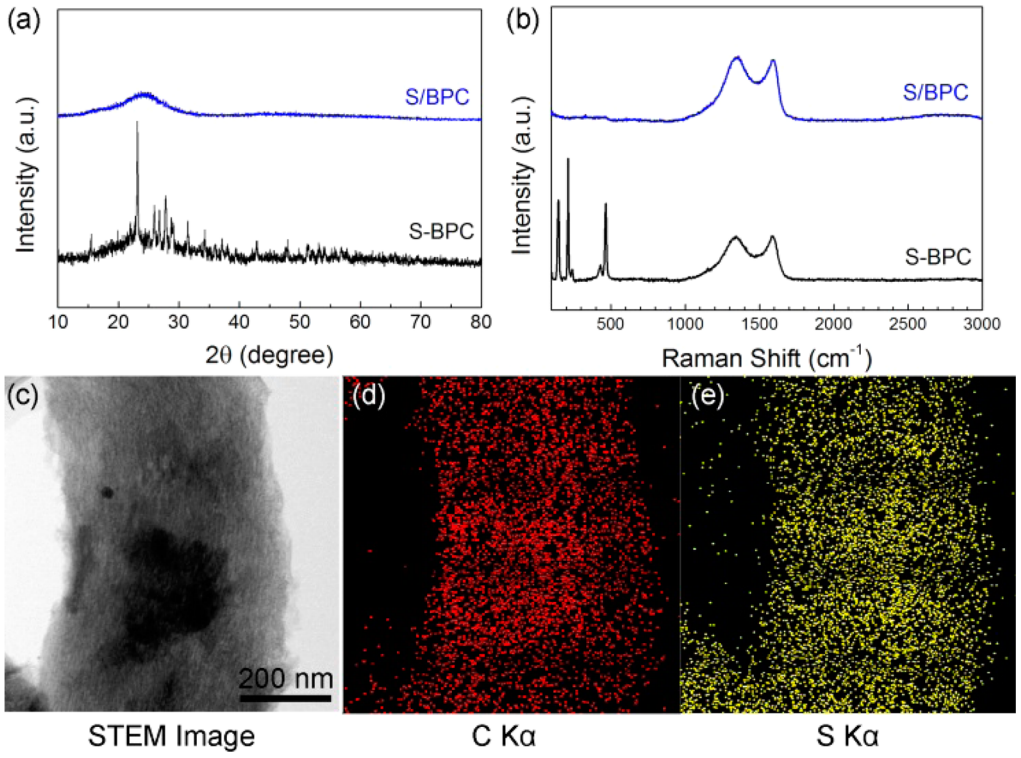

Figure 2. (a) XRD patterns and (b) Raman spectra of S-BPC mixture and S/BPC composite; (c) bright field STEM image and corresponding (d) C and (e) S EDX elemental mappings of a S/BPC particle.

NaOH solution for 2 h at 60 °C. The as-prepared BPC was collected by centrifugation, repeatedly washed by deionized water, and finally dried in an oven.

In addition, undoped porous carbon CMK-3 and nitrogen-doped porous carbon (NPC) were also synthesized for comparison. CMK-3 was prepared using the method in a previous paper.[40] NPC was derived from urea resin with SBA-15 template. In a typical preparation, urea (Xilong Chemical Co. Ltd.) was dissolved in formaldehyde (Xilong Chemical Co. Ltd.) with a molar ratio of 1:1.05, forming a concentrated solution. SBA-15 was immersed in the solution and sonicated for 1 h. After adjustment to pH 2 with 1 M HCl solution, urea and formaldehyde reacted for 1 h to yield urea resin inside the mesopores of SBA-15. The precursor was heated at 100 °C for 12 h, followed by 160 °C for another 12 h. NPC was obtained by carbonizing the intermediate at 900 °C for 5 h in Ar and finally removing the silica template.

Synthesis of Sulfur/Carbon Composite. S/BPC, S/CMK-3, and S/NPC were all prepared by the same method. S (Sigma-Aldrich, Co.) and porous carbon were mixed with a mass ratio of 7:3 and then sealed in a glass tube filled with Ar. The sealed glass was annealed at 400 °C in a tube furnace for 5 h. Most of the S diffused into the pores of carbon, but a small amount of S might adhere to the tube wall and the surface of carbon. S on the surface of C was further removed at 220 °C for 6 h, obtaining the final S/C composite.

2.2. Material Characterizations. A field emission scanning electron microscope (SEM, JEOL 6701F) was used to investigate the morphologies, particle sizes of the samples. Transmission electron microscopy and elemental compositions of the samples were determined by JEM-2100F (JEOL) coupled with an energy-dispersive X-ray spectroscopy (EDX, Phoenix) system. Wide-angle and low-angle X-ray powder diffraction (XRD) of the as-obtained samples were recorded on a Rigaku D/max-2500 with Cu Kα radiation (λ = 1.540 56 Å) operated at 40 kV and 200 mA. Raman measurements were performed using a DXR from Thermo Scientific with a laser wavelength of 532 nm. To calculate the pore size distribution and pore volumes, the nitrogen absorption and desorption isotherms were measured at 77.3 K with an Autosorb-1 specific surface area analyzer from Quantachrome. The content of N in N-doped porous carbon was determined by NHC elemental analysis using Flash EA 1112. Thermogravimetric (TG) analysis of S/C composite was performed on TG/DTA 6300 in an N_2 flow to obtain the S content in the composite.

A four-contact method was applied to measure the powder electronic conductivity of porous carbons. The powder sample was pressed to disk at 4 MPa with two stainless-steel plungers, whose resistance was measured by a Keithley 2400 digital multimeter in four-wire mode. The conductivity of the sample was calculated according to the resistance and the size of the disk.

Information of the surface elements was obtained by X-ray photoelectron spectroscopy (XPS) performed on the Thermo Scientific ESCALab 250Xi using 200 W monochromatic Al Kα radiation. The 500 μm X-ray spot was used for XPS analysis. The base pressure in the analysis chamber was about 3 × 10^{-10} mbar. All reported data of XPS binding energy are calibrated based on the hydrocarbon C 1s line at 284.8 eV from adventitious carbon. Spectra were fitted with Lorentzian−Gaussian functions and smart background using Thermo Avantage software.

2.3. Electrochemical Characterizations. The positive electrodes were composed of S/C composite, super P, and poly(vinyl difluoride) (PVDF) binder with a weight ratio of 8:1:1, which were coated onto an Al foil and dried at 60 °C overnight. Li−S batteries were assembled in CR2032 coin cells in an argon-filled glovebox by using glass fiber from Whatman as separator and lithium foil as the anode. The electrolyte was 1 M lithium bis(trifluoromethane) sulfonimide (LiTFSI) in 1,3-dioxolane/dimethoxymethane (DOL/DME, 1:1 by volume) (Zhangjiagang Guotaihuarong New Chemical Materials Co., Ltd.). Galvanostatic discharge/charge voltage profiles of the assembled cells were performed on a LAND system in the voltage range of 1.0−2.7 V (vs Li^+/Li). Cyclic voltammogram (CV) test was carried out using an Autolab PG302 N electrochemical workstation from 1.0 to 2.7 V (vs Li^+/Li) at a sweep rate of 0.1 mV/s. Electrochemical impedance spectra (EIS) measurement was also performed on the Autolab workstation with frequency range from 100 kHz to 100 mHz.

dx.doi.org/10.1021/am501627f | ACS Appl. Mater. Interfaces 2014, 6, 8789−8795

The C-rate used was based on the theoretical capacity of S (1675 mA h g^{-1}). All electrochemical measurements were carried out at 25 °C.

3. RESULTS AND DISCUSSION

Derived from the SBA-15 template, BPC has uniform size and ordered pore structure, as evident from the SEM (Figure 1a) and TEM (Figure 1b) images. The pore structure is further proven to be ordered by the low-angle XRD (Figure 1c). Analysis of the N_2 isotherm adsorption/desorption and pore size (Figure 1d) indicates that mesopores contribute to the majority of the pore volume of BPC, while micropores contribute to a small portion. The total pore volume of BPC is 1.4 cm^3 g^{-1}, which favors high-S-content accommodation. To confirm that the carbon material is indeed doped with B atoms, we carried out XPS for elemental analysis. According to the B 1s XPS spectrum (Figure 1e), B is present in BPC mainly as BCO_2, BC_2O, and BC_3 species.[37] A residual amount of B_2O_3 from the raw material H_3BO_3 is also identified. This proves that major B is incorporated into the backbone of carbon (Figure 1f). The content of B dopant in BPC is 0.93 atom % according to XPS. The XPS elemental analysis indicates that B dopant has modified the surface chemistry of the carbon substrate, the effect of which is discussed in detail below.

For the preparation of S/BPC composite, S was infiltrated into the pores of BPC at 400 °C. The characteristic XRD peaks of orthorhombic S and Raman peaks of S_8 in S-BPC disappear after S is impregnated into the BPC (Figure 2a and Figure 2b), which indicates that the crystalline S has transformed to amorphous S embedded in BPC. Consistently, no bulk-sized S can be observed in the SEM image of S/BPC (Figure S1 in Supporting Information). Scanning transmission electron microscopy (STEM) image and elemental mappings (Figure 2c–e) further demonstrate the homogeneous distribution of S in the porous carbon. The content of S in S/BPC is 53 wt % according to TG analysis (Figure S2).

To specifically disclose the effect of the dopant on the carbon and S/C composite while excluding the impact of the morphology, structure, and porosity of carbon materials, undoped mesoporous carbon CMK-3 and N-doped porous carbon (NPC) were also prepared from the same SBA-15 template as the control materials. As shown in Figures 1, S3, and S4, BPC, CMK-3, and NPC exhibit analogous morphology and porosity. In addition, Raman spectra of CMK-3, NPC, and BPC were collected to show their crystallinity (Figure S5), where the intensity ratios of G-band and D-band are almost identical. This indicates that graphitization degrees of these carbon materials are similar. Thus, any observed differences in the physical and chemical properties of these three carbon materials should be assigned to the heteroatomic dopants. As listed in Table 1, NPC, with 5.96 atom % N by XPS analysis (or 8.3 wt % by NHC elemental analysis), presents the highest conductivity. The electronic conductivity of BPC, even with only 0.93 atom % B, is higher when compared with undoped CMK-3. Such increase in the conductivity is in favor of the electrochemical activity of S.

Table 1. Content of Heteroatoms in Carbon Materials and Electric Conductivity of CMK-3, NPC, and BPC

	CMK-3	NPC	BPC
heteroatom content (atom % by XPS)	0	5.96	0.93
conductivity (S cm^{-1})	0.13	1.10	0.42

While B and N dopants share the ability to improve the conductivity of carbon materials, B and N in carbon framework function in different ways. In contrast to N, B has a lower electronegativity than C, so B atoms are positively polarized, leading to chemisorption of negative species on the surface of BPC.[37] As S and polysulfide anions are electron abundant, they can be attracted by the slightly positive B. To confirm the interaction between S and BPC, we synthesized S/CMK-3, S/NPC, and S/BPC composites under the same condition. From the S 1s XPS spectra of these S/C composites (Figure 3), we

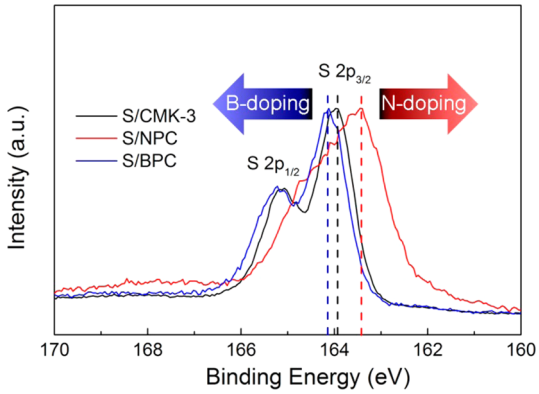

Figure 3. S 2p XPS spectra analysis of S/CMK-3, S/NPC, and S/BPC.

can see that the binding energy of S in S/BPC is higher than that of S in S/CMK-3 and S/NPC. This implies that the electron density of S slightly transfers toward the carbon framework, leading to the interaction between S and BPC. For polysulfide S_x^{2-} (x = 4–8) anions, the Coulombic interaction would be even stronger, and polysulfide anions can therefore be entrapped within the cathode. However, in neutral CMK-3 and electron-abundant NPC, no such chemisorption occurs. Thus, B-doped carbon materials can offer a unique advantage over undoped and N-doped materials, i.e., polysulfide adsorption for stable Li–S batteries.

Electrochemical evaluation demonstrates the significant role of B dopant in S/C composite cathode. To place emphasis on investigating the effect of the cathode, we neither modified the electrolyte (1 M LiTFSI in DOL/DME) with additives[41] nor modified the battery configuration (with carbon interlayers).[42] Cycle voltammogram (Figure 4a), in agreement with the discharge/charge voltage profile (Figure 4b), reveals the reduction peaks at 2.4 and 2.0 V, which are the typical output voltages of Li–S batteries. Additionally, a reduction peak at 1.7 V is also observed, which originates from the S filled in the micropores.[22] The galvanostatic discharge/charge voltage profile (Figure 4b) displays a high first discharge capacity of ~1300 mA h g^{-1} (based on the mass of S), indicating the high activity of S in BPC. After a charging to 2.7 V, the Coulombic efficiency approaches 100%; the shuttle effect is obviously alleviated. As we know, for Li–S batteries, the shuttle effect causes severe capacity decay. Therefore, the discharge capacity of S/CMK-3 decreases rapidly from 984 mA h g^{-1} in the first cycle to <250 mA h g^{-1} in the 80th cycle (Figure 5a). Even though N doping is reported to be beneficial for cycling stability and the optimal N content is 8.3 wt % for S/C cathode,[35,36] the S/NPC composite is still plagued with the capacity decline as shown in Figure 5a, especially during the first several cycles. The likely reason for this decline can be ascribed to the shuttle effect of polysulfide anions, which are

dx.doi.org/10.1021/am501627f | ACS Appl. Mater. Interfaces 2014, 6, 8789–8795

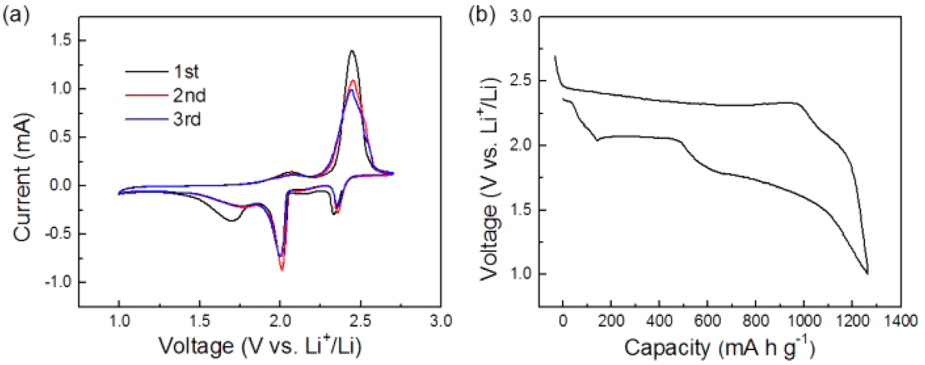

Figure 4. (a) Cycle voltammogram of S/BPC at sweep rate of 0.1 mV s^{-1}; (b) initial galvanostatic discharge/charge voltage profile of S/BPC.

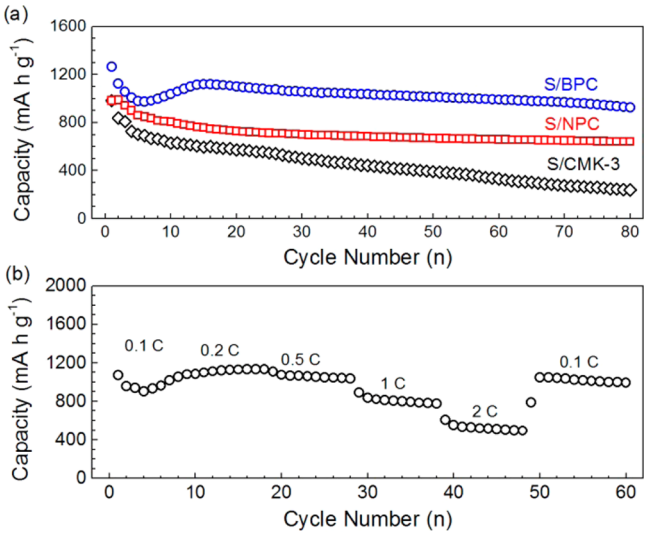

Figure 5. (a) Discharge capacities of S/CMK-3, S/NPC, and S/BPC at C/4; (b) discharge capacities of S/BPC at different current rates.

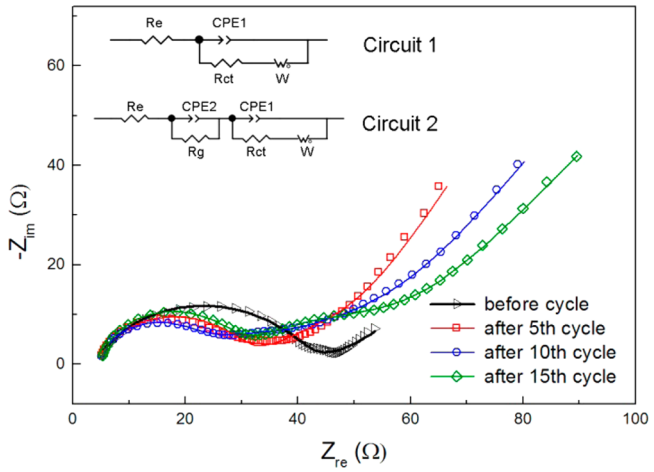

Figure 6. Nyquist plots for the S/BPC before electrochemical cycling and after different cycles charging to 2.7 V (dots, experimental data; lines, simulated data). The insets are the equivalent circuits used to fit the impedance spectra (circuit 1 for data before cycle, circuit 2 for data after different cycles).

dissolved in the electrolyte and shuttle to the anode, causing S loss. Superior to undoped CMK-3 and NPC, BPC has the benefit of trapping polysulfide anions. Therefore, S/BPC exhibits a more stable cycling performance. In S/BPC cathode, though the polysulfide anions dissolve in the electrolyte in the initial few cycles (as in S/CMK-3 and S/NPC), the polysulfide anions are generally aggregated and adsorbed by the positive polarized B in BPC. The polysulfide anions at the cathode side, known as "catholyte", are electrochemically active and contribute to the capacity.[5] As a result, after the initial decrease, the discharge capacity increases after the initial decrease and stabilizes to >900 mA h g^{-1} after 80 cycles, which demonstrates the favorable cyclability of S/BPC. In addition, S/BPC also exhibits excellent rate capability. S/BPC delivers approximately 1000, 800, and 500 mA h g^{-1} at 0.5, 1, and 2 C, respectively (Figure 5b). A capacity of >1000 mA h g^{-1} is regained right after the current density recovers to 0.1 C. The remarkable electrochemical performance of S/BPC, benefiting from B doping, guarantees its feasible application in Li−S batteries.

To further exhibit the effect of B doping on the interfacial resistance in the batteries, we measured the EIS data of S/BPC after different cycles (Figure 6). EIS of S/CMK-3 is also shown for comparison (Figure S6). The electrochemical impedance data are fitted according to two equivalent circuits that are used to simulate the electrochemical models of the Li−S battery.[25,43] The parameters derived from the simulation are summarized in Table S1. Charge-transfer resistance (R_{ct}) of S/BPC (36.6 Ω) is much lower than that of S/CMK-3 (65.6 Ω), which elucidates the improved conductivity of B-doped carbon compared with the undoped one. During the electrochemical reaction, there is a moderate increase in R_g; this is related to the growth of the trace amount of Li_2S (or Li_2S_2), which is not converted to S during the charging process. A close examination of the parameters within cycling reveals that the Warburg impedance increases in the first 10 cycles and then decreases after 15 cycles (Table S1). As Warburg impedance in Li−S batteries is associated with the diffusion of the polysulfides,[43] this change indicates that polysulfide anions are first dissolved in the electrolyte and then are gradually trapped by BPC. The evolution of Warburg impedance, consistent with the cycling performance of S/BPC (Figure 5a), provides another proof for the ability of BPC to confine polysulfide anions.

4. CONCLUSIONS

In summary, B doping plays an important role in improving the performance of S/C cathode in Li−S batteries. On one hand, doping with B increases the conductivity of porous carbon. Therefore, B-doped S/C cathode displays enhanced rate performance and reduced battery resistance. On the other hand, B atoms in carbon framework possess a partial positive charge. This polarized surface can chemically adsorb the negative polysulfides. Therefore, B dopant in S/C cathode

dx.doi.org/10.1021/am501627f | ACS Appl. Mater. Interfaces 2014, 6, 8789−8795

constrains the dissolved polysulfide anions to the cathode side and enhances the cycling stability of batteries. Owing to the improved conductivity and polysulfide chemisorption effects, S/BPC delivers a reversible capacity of >900 mA h g^{-1} after 80 cycles and a superior rate performance. Aiming to reveal the effect of B dopant on S/C cathode, we simply adopted porous carbon materials as model system without further structure design in this work. Considering the unique advantages of B-doped carbon materials, we believe that the high energy density of S cathode will be exploited within a rational structure and optimized content of B. The strategy of doping carbon with B can also be instructive for developing energy related carbon materials.

■ ASSOCIATED CONTENT

Supporting Information

SEM image and TG analysis of S/BPC; TEM images, pore size, XPS analysis of CMK-3 and NPC; Raman spectra of CMK-3, NPC, and BPC; EIS Nyquist plot of S/CMK-3 and fitted parameters of EIS data. This material is available free of charge via the Internet at http://pubs.acs.org.

■ AUTHOR INFORMATION

Corresponding Author

*E-mail: ygguo@iccas.ac.cn. Phone/Fax: (+86) 10-82617069.

Notes

The authors declare no competing financial interest.

■ ACKNOWLEDGMENTS

This work was supported by the "Strategic Priority Research Program" of the Chinese Academy of Sciences (Grant XDA09010300), the National Natural Science Foundation of China (Grants 51225204, 91127044, 21121063, and U1301244), the National Basic Research Program of China (Grants 2011CB935700, 2012CB932900, and 2013AA050903), and the Chinese Academy of Sciences.

■ REFERENCES

(1) Goodenough, J. B. Electrochemical Energy Storage in a Sustainable Modern Society. *Energy Environ. Sci.* **2014**, *7*, 14−18.

(2) Wang, Y.; Cao, G. Developments in Nanostructured Cathode Materials for High-Performance Lithium-Ion Batteries. *Adv. Mater.* **2008**, *20*, 2251−2269.

(3) Liu, B.; Zhang, J.; Wang, X.; Chen, G.; Chen, D.; Zhou, C.; Shen, G. Hierarchical Three-Dimensional $ZnCo_2O_4$ Nanowire Arrays/Carbon Cloth Anodes for a Novel Class of High-Performance Flexible Lithium-Ion Batteries. *Nano Lett.* **2012**, *12*, 3005−3011.

(4) Hu, L.; Chen, W.; Xie, X.; Liu, N.; Yang, Y.; Wu, H.; Yao, Y.; Pasta, M.; Alshareef, H. N.; Cui, Y. Symmetrical MnO_2−Carbon Nanotube−Textile Nanostructures for Wearable Pseudocapacitors with High Mass Loading. *ACS Nano* **2011**, *5*, 8904−8913.

(5) Ji, X.; Nazar, L. F. Advances in Li−S Batteries. *J. Mater. Chem.* **2010**, *20*, 9821−9826.

(6) Bruce, P. G.; Freunberger, S. A.; Hardwick, L. J.; Tarascon, J. M. Li−O_2 and Li−S Batteries with High Energy Storage. *Nat. Mater.* **2012**, *11*, 19−29.

(7) Manthiram, A.; Fu, Y.; Su, Y.-S. Challenges and Prospects of Lithium−Sulfur Batteries. *Acc. Chem. Res.* **2012**, *46*, 1125−1134.

(8) Evers, S.; Nazar, L. F. New Approaches for High Energy Density Lithium−Sulfur Battery Cathodes. *Acc. Chem. Res.* **2012**, *46*, 1135−1143.

(9) Yin, Y.-X.; Xin, S.; Guo, Y.-G.; Wan, L.-J. Lithium−Sulfur Batteries: Electrochemistry, Materials, and Prospects. *Angew. Chem., Int. Ed.* **2013**, *52*, 13186−13200.

(10) Ye, H.; Yin, Y.-X.; Xin, S.; Guo, Y.-G. Tuning the Porous Structure of Carbon Hosts for Loading Sulfur toward Long Lifespan Cathode Materials for Li−S Batteries. *J. Mater. Chem. A* **2013**, *1*, 6602−6608.

(11) Li, X.; Cao, Y.; Qi, W.; Saraf, L. V.; Xiao, J.; Nie, Z.; Mietek, J.; Zhang, J.-G.; Schwenzer, B.; Liu, J. Optimization of Mesoporous Carbon Structures for Lithium−Sulfur Battery Applications. *J. Mater. Chem.* **2011**, *21*, 16603−16610.

(12) Ji, X.; Lee, K.; Nazar, L. A Highly Ordered Nanostructured Carbon−Sulphur Cathode for Lithium−Sulphur Batteries. *Nat. Mater.* **2009**, *8*, 500−506.

(13) Jayaprakash, N.; Shen, J.; Moganty, S. S.; Corona, A.; Archer, L. A. Porous Hollow Carbon@Sulfur Composites for High-Power Lithium−Sulfur Batteries. *Angew. Chem., Int. Ed.* **2011**, *50*, 5904−5908.

(14) Xu, T.; Song, J.; Gordin, M.; Sohn, H.; Yu, Z.; Chen, S.; Wang, D. Mesoporous Carbon−Carbon Nanotube−Sulfur Composite Microspheres for High-Areal-Capacity Lithium−Sulfur Battery Cathodes. *ACS Appl. Mater. Interfaces* **2013**, *5*, 11355−11362.

(15) Ji, L.; Rao, M.; Aloni, S.; Wang, L.; Cairns, E. J.; Zhang, Y. Porous Carbon Nanofiber−Sulfur Composite Electrodes for Lithium/Sulfur Cells. *Energy Environ. Sci.* **2011**, *4*, 5053−5059.

(16) Zu, C.; Manthiram, A. Hydroxylated Graphene−Sulfur Nanocomposites for High-Rate Lithium−Sulfur Batteries. *Adv. Energy Mater.* **2013**, *3*, 1008−1012.

(17) Guo, J.; Xu, Y.; Wang, C. Sulfur-Impregnated Disordered Carbon Nanotubes Cathode for Lithium−Sulfur Batteries. *Nano Lett.* **2011**, *11*, 4288−4294.

(18) Zheng, G.; Yang, Y.; Cha, J. J.; Hong, S. S.; Cui, Y. Hollow Carbon Nanofiber-Encapsulated Sulfur Cathodes for High Specific Capacity Rechargeable Lithium Batteries. *Nano Lett.* **2011**, *11*, 4462−4467.

(19) Zhang, C.; Wu, H. B.; Yuan, C.; Guo, Z.; Lou, X. W. D. Confining Sulfur in Double-Shelled Hollow Carbon Spheres for Lithium−Sulfur Batteries. *Angew. Chem., Int. Ed.* **2012**, *51*, 9592−9595.

(20) Wang, D. W.; Zhou, G.; Li, F.; Wu, K. H.; Lu, G. Q.; Cheng, H. M.; Gentle, I. R. A Microporous−Mesoporous Carbon with Graphitic Structure for a High-Rate Stable Sulfur Cathode in Carbonate Solvent-Based Li−S Batteries. *Phys. Chem. Chem. Phys.* **2012**, *14*, 8703−8710.

(21) Lu, S.; Cheng, Y.; Wu, X.; Liu, J. Significantly Improved Long-Cycle Stability in High-Rate Li−S Batteries Enabled by Coaxial Graphene Wrapping over Sulfur-Coated Carbon Nanofibers. *Nano Lett.* **2013**, *13*, 2485−2489.

(22) Xin, S.; Gu, L.; Zhao, N. H.; Yin, Y. X.; Zhou, L. J.; Guo, Y. G.; Wan, L. J. Smaller Sulfur Molecules Promise Better Lithium−Sulfur Batteries. *J. Am. Chem. Soc.* **2012**, *134*, 18510−18513.

(23) Lee, J. T.; Zhao, Y.; Thieme, S.; Kim, H.; Oschatz, M.; Borchardt, L.; Magasinski, A.; Cho, W. I.; Kaskel, S.; Yushin, G. Sulfur-Infiltrated Micro- and Mesoporous Silicon Carbide-Derived Carbon Cathode for High-Performance Lithium Sulfur Batteries. *Adv. Mater.* **2013**, *25*, 4573−4579.

(24) Weng, W.; Pol, V. G.; Amine, K. Ultrasound Assisted Design of Sulfur/Carbon Cathodes with Partially Fluorinated Ether Electrolytes for Highly Efficient Li/S Batteries. *Adv. Mater.* **2013**, *25*, 1608−1615.

(25) Zhang, B.; Qin, X.; Li, G. R.; Gao, X. P. Enhancement of Long Stability of Sulfur Cathode by Encapsulating Sulfur into Micropores of Carbon Spheres. *Energy Environ. Sci.* **2010**, *3*, 1531−1537.

(26) Xu, G.-L.; Xu, Y.-F.; Fang, J.-C.; Peng, X.-X.; Fu, F.; Huang, L.; Li, J.-T.; Sun, S.-G. Porous Graphitic Carbon Loading Ultra High Sulfur as High-Performance Cathode of Rechargeable Lithium-Sulfur Batteries. *ACS Appl. Mater. Interfaces* **2013**, *5*, 10782−10793.

(27) Kim, J.; Lee, D.-J.; Jung, H.-G.; Sun, Y.-K.; Hassoun, J.; Scrosati, B. An Advanced Lithium−Sulfur Battery. *Adv. Funct. Mater.* **2013**, *23*, 1076−1080.

(28) Demir-Cakan, R.; Morcrette, M.; Nouar, F.; Davoisne, C.; Devic, T.; Gonbeau, D.; Dominko, R.; Serre, C.; Ferey, G.; Tarascon, J. M. Cathode Composites for Li−S Batteries via the Use of Oxygenated Porous Architectures. *J. Am. Chem. Soc.* **2011**, *133*, 16154−16160.

(29) Zheng, G.; Zhang, Q.; Cha, J.; Yang, Y.; Li, W.; Seh, Z.; Cui, Y. Amphiphilic Surface Modification of Hollow Carbon Nanofibers for

Improved Cycle Life of Lithium Sulfur Batteries. *Nano Lett.* **2013**, *13*, 1265−1270.
(30) Paraknowitsch, J. P.; Thomas, A. Doping Carbons beyond Nitrogen: An Overview of Advanced Heteroatom Doped Carbons with Boron, Sulphur and Phosphorus for Energy Applications. *Energy Environ. Sci.* **2013**, *6*, 2839−2855.
(31) Wolfgang, S. Solid-State Chemistry with Nonmetal Nitrides. *Angew. Chem., Int. Ed.* **1993**, *32*, 806−818.
(32) Zhang, K.; Han, P.; Gu, L.; Zhang, L.; Liu, Z.; Kong, Q.; Zhang, C.; Dong, S.; Zhang, Z.; Yao, J.; Xu, H.; Cui, G.; Chen, L. Synthesis of Nitrogen-Doped MnO/Graphene Nanosheets Hybrid Material for Lithium Ion Batteries. *ACS Appl. Mater. Interfaces* **2012**, *4*, 658−664.
(33) Li, X.; Geng, D.; Zhang, Y.; Meng, X.; Li, R.; Sun, X. Superior Cycle Stability of Nitrogen-Doped Graphene Nanosheets as Anodes for Lithium Ion Batteries. *Electrochem. Commun.* **2011**, *13*, 822−825.
(34) Li, X.; Liu, J.; Zhang, Y.; Li, Y.; Liu, H.; Meng, X.; Yang, J.; Geng, D.; Wang, D.; Li, R.; Sun, X. High Concentration Nitrogen Doped Carbon Nanotube Anodes with Superior Li^+ Storage Performance for Lithium Rechargeable Battery Application. *J. Power Sources* **2012**, *197*, 238−245.
(35) Sun, X.-G.; Wang, X.; Mayes, R.; Dai, S. Lithium−Sulfur Batteries Based on Nitrogen-Doped Carbon and an Ionic-Liquid Electrolyte. *ChemSusChem* **2012**, *5*, 2079−2085.
(36) Sun, F.; Wang, J.; Chen, H.; Li, W.; Qiao, W.; Long, D.; Ling, L. High Efficiency Immobilization of Sulfur on Nitrogen-Enriched Mesoporous Carbons for Li−S Batteries. *ACS Appl. Mater. Interfaces* **2013**, *5*, 5630−5638.
(37) Yang, L.; Jiang, S.; Zhao, Y.; Zhu, L.; Chen, S.; Wang, X.; Wu, Q.; Ma, J.; Ma, Y.; Hu, Z. Boron-Doped Carbon Nanotubes as Metal-Free Electrocatalysts for the Oxygen Reduction Reaction. *Angew. Chem., Int. Ed.* **2011**, *50*, 7132−7135.
(38) Wang, D.-W.; Li, F.; Chen, Z.-G.; Lu, G. Q.; Cheng, H.-M. Synthesis and Electrochemical Property of Boron-Doped Mesoporous Carbon in Supercapacitor. *Chem. Mater.* **2008**, *20*, 7195−7200.
(39) Han, J.; Zhang, L. L.; Lee, S.; Oh, J.; Lee, K.-S.; Potts, J. R.; Ji, J.; Zhao, X.; Ruoff, R. S.; Park, S. Generation of B-Doped Graphene Nanoplatelets Using a Solution Process and Their Supercapacitor Applications. *ACS Nano* **2012**, *7*, 19−26.
(40) Yang, C.-P.; Xin, S.; Yin, Y.-X.; Ye, H.; Zhang, J.; Guo, Y.-G. An Advanced Selenium−Carbon Cathode for Rechargeable Lithium−Selenium Batteries. *Angew. Chem., Int. Ed.* **2013**, *52*, 8363−8367.
(41) Zhang, S. S. Role of $LiNO_3$ in Rechargeable Lithium/Sulfur Battery. *Electrochim. Acta* **2012**, *70*, 344−348.
(42) Su, Y. S.; Manthiram, A. Lithium−Sulphur Batteries with a Microporous Carbon Paper as a Bifunctional Interlayer. *Nat. Commun.* **2012**, *3*, 1166.
(43) Yuan, L.; Qiu, X.; Chen, L.; Zhu, W. New Insight into the Discharge Process of Sulfur Cathode by Electrochemical Impedance Spectroscopy. *J. Power Sources* **2009**, *189*, 127−132.